Proceedings of the Fortieth Turbomachinery Symposium
September 12-15, 2011, Houston, Texas

FULL LOAD TESTING OF A 12.5MW VERTICAL HIGH SPEED SUBSEA MOTORCOMPRESSOR

Giuseppe Vannini
Senior Engineer (Mechanical Engineer)
GE Oil&Gas Nuovo Pignone
Via Felice Matteucci, 2, 50127, Florence, Italy

Andrea Masala
Senior Engineer (Mechanical Engineer)
GE Oil&Gas, Nuovo Pignone
Via Felice Matteucci, 2, 50127, Florence, Italy

Massimiliano Ortiz Neri
Lead Engineer (Control Engineer)
GE Oil&Gas, Nuovo Pignone
Via Felice Matteucci, 2, 50127, Florence, Italy

Silvia Evangelisti
Lead Engineer (Test Project Engineer)
GE Oil&Gas, Nuovo Pignone
Via Felice Matteucci, 2, 50127, Florence, Italy

Massimo Camatti
Engineering Manager
GE Oil&Gas, Nuovo Pignone
Via Felice Matteucci, 2, 50127, Florence, Italy

Federico Svetti
Lead Engineer (Electrical Engineer)
GE Oil&Gas, Nuovo Pignone
Via Felice Matteucci, 2, 50127, Florence, Italy

Sergio Bondi
Principal Engineer (System Engineer)
GE Oil&Gas, Nuovo Pignone
Via Felice Matteucci, 2, 50127, Florence, Italy

Giuseppe Vannini is a Senior Engineer in the Advanced Technology Organization of GE Oil&Gas, which he joined in early 2001. He has been involved in advanced rotordynamics studies on high performance compressors developing both analytical and experimental research activities. Recently he extended his activity to the design of prototypes for subsea applications (i.e. integrated high speed motocompressors). He holds a PhD in Mechanical Engineering at Pisa University and he's member of API684 Task Force.

Andrea Masala is Senior Engineer in GE Oil&Gas Advanced Technology Rotordynamic team. He earned is MSc in Mechanical Engineering from University of Cagliari in 1999 and joined GE in 2002. He had assignments in the auxiliaries systems, rotating machinery and centrifugal compressors NPI teams. In the current position his area of activity is on rotating equipment dynamics with focus on AMBs integration in GE Oil&Gas machines. He is a certified Root Cause Analysis leader and Six Sigma DFSS green belt.

Masimiliano Ortiz Neri graduated in Automation Engineering from the University of Pisa in 1999. After several years of work in the telecommunication industry, he joined GE Oil&Gas in 2005 as Control Systems engineer in the Steam Turbine and Electric Motor Driven Turbomachinery Control Department, being involved in the design of the control system for several challenging NPI projects like Subsea Compressor and Solar Power Plant. He is specialized in Active Magnetic Bearing control system.

Silvia Evangelisti is a Lead Test Engineer in GE Oil&Gas Technology Laboratory. She joined GE in 2001, and moved to her current role in 2005, after Engineering Edison Development Program. She has been involved in several projects, from conceptual test design
to data analysis, with a special focus on centrifugal compressors validation area. Silvia holds a M.S. degree in Mechanical Engineering from the University of Bologna.

Massimo Camatti is the manager of Turbomachinery Mechanical Design Dpt. of Advanced Technology Division of GE Oil&Gas. He holds a Master Degree in Mechanical Engineering at Florence University and joined Nuovo Pignone in 1988. After a first period as centrifugal compressors design engineer he was design leader of innovative compression projects. Before the current position, he covered the roles of engineering manager of centrifugal and axial compressors for Liquefied Natural Gas application and R&D manager for centrifugal and axial compressor product line.

Federico Svetti is an Engineering Technical Leader in the Electrical & Control System Department of GE Oil & Gas, Florence. He joined the company in the 2006 and, since that time, he has followed the design of electrical drives (Variable Speed Drive Systems) for Motor-compressors and LNG applications. In the last 2 years, he has been involved in the new technologies and applications around the subsea field.
He received the MSc. in Electrical Engineering from the University of Pisa, Italy, in 2002.

Sergio Bondi started his career in the aerospace sector and then moved to Oil&Gas. He developed his expertise within rotating machinery with special focus in gear and couplings and then took the responsibility of the system integration of the subsea compressor. Currently he his responsible for pumps, valves and systems manufactured by GE Oil&Gas. He is graduated in aeronautical engineering and holds an MBA from Bocconi University.

ABSTRACT

In late 2006 Authors' Company was awarded a contract for the motorcompressor for the Ormen Lange Subsea Compression Pilot. This Pilot represents the first subsea motorcompressor unit ever built in a fully marinized version and tested in a water pit, which was developed specifically for the project at the customer's site (Nhyamna, Norway).

The prototype unit is a 12.5MW (16763HP) integrated motorcompressor, which runs up to 10.5krpm in a vertical configuration with the following features:

- Single casing
- High-speed motor rigidly coupled to a multistage centrifugal compressor (3 journal bearings shaft line)
- Canned Active Magnetic Bearings (AMBs)
- Process gas used as cooling fluid for the Electric Motor
- Internal separation system (to protect the bearings and the electric motor from the intrusion of solid and liquid materials)
- Fully marinized AMBs control system
- The design and validation plan for this complex equipment were developed through a four years program where many challenging milestones were achieved.
- The Ormen Lange Subsea Compression Pilot motorcompressor has successfully completed an intensive full load testing campaign in the Authors' Company plant including the following:
- Static-dynamic tuning of the AMBs
- Mechanical Running Test
- Compressor Performance Test (ASME PTC-10 Type 2 + Full Load test)
- Electric Motor Performance Test
- Overall cooling system check
- Landing test (partial landing and full speed delevitation test)

The test campaign has fully demonstrated the functionality of this prototype unit capable of operation in the service conditions.

The Next step will be the shipment to the costumer site where the submerged testing will be conducted.

This paper will provide a detailed description of the main test results of the subsea motorcompressor covering all aspects of the test program including rotordynamic behaviour, compressor thermodynamic performance, axial load variation versus operating conditions (monitored thanks to the thrust AMB), electric motor cooling system behaviour, electric motor performance, AMBs and control system operability.

Of special interest is the rotor delevitation test from full speed consisting in the two ton rotor running at 10.5krpm dropping onto the mechanical emergency bearings until the machine reached a complete stop condition. This test, which was repeated 5 times, provided a full-scale verification of the landing numerical simulation developed by the authors (Ransom et al., 2009).

INTRODUCTION

In 2006 the Authors' Company was awarded a contract for the motorcompressor of the Ormen Lange Subsea Compression pilot project. Soon after, the Authors' Company (together with the project EPC) started the long and demanding task of delivering this subsea motorcompressor suitable for uninterrupted operation on the bed of the North Sea.

The project centers on the development of a complete compression train to demonstrate the feasibility of subsea technology through extensive testing in the Nyhamna pit. The Pilot compression train delivered to the final costumer (HydroStatoil) will be in fact tested in a specially constructed test facility (Nyhamna site) where a special pit will be prepared to simulate subsea conditions.

The Pilot compression train (see Figure 1) includes:

- Motocompressor unit
- AMBs control system
- Upstream separator
- Subsea Variable Speed Driver
- Subsea Ancillaries: condensate pump, transformers, circuit breakers.

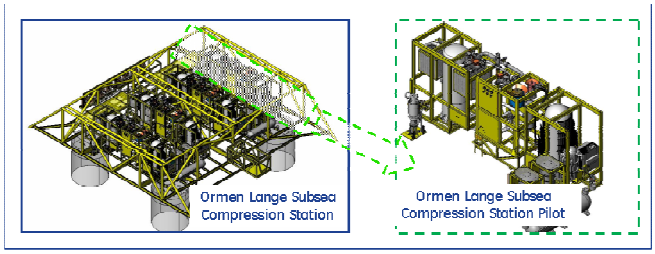

Figure 1 – Ormen Lange subsea compressor station.

The Ormen Lange Subsea Compression Pilot project will be the enabler for the Ormen Lange production phase, which will employ four trains (identical to the Pilot) in subsea service.

This motorcompressor was developed over a four full year period (from design to testing) and is a full prototype for the subsea compression service. During this time, the project achieved many important milestones in terms of qualification of technology for the various single components. These achievements will not be covered in detail in this article, which is dedicated primarily to the full load testing of the unit but it is worthwhile to mention them as background.

The emergency landing of a vertical shaft on three journal bearings was validated through a subscale test done in the laboratory (Ransom et al., 2009). This test increased the confidence in the design of the bearings and also served as a demonstration of the smooth operation of the vertical shaft on the AMBs.

Still on rotordynamics, the high speed balancing of the three-journal bearing rotor was performed at the Authors' Company plant to guarantee smooth vibration behaviour during the full load test. The balancing operation was very challenging due to the need for three supports and the high peripheral speeds reached at the bearings (160m/sec – 525ft/sec).

Other important milestones were achieved in the development of canned AMBs, marinized control system validation and electric motor stator parts qualification for a wet environment and erosion.

In the following paragraphs, the functional testing of all these components assembled together will be discussed in detail.

Before entering into the details of the test program it is

worthy to describe the motocompressor layout, which is shown in Figure 2.

The unit is a vertical integrated motorcompressor running up to 10.5krpm and rated for 12.5MW of power. The electric motor is located topside and it is housed in a cast stainless steel casing, which provides interfaces for the high voltage connectors. The rotor is a single shaft line thanks to the rigid Hirth coupling and is supported by three radial AMBs.

The following discussion provides some more specific thoughts on the main features of the motorcompressor. The vertical layout based on the topside electric motor was selected for this application with the specific goal of protecting the electric motor from water and condensates.

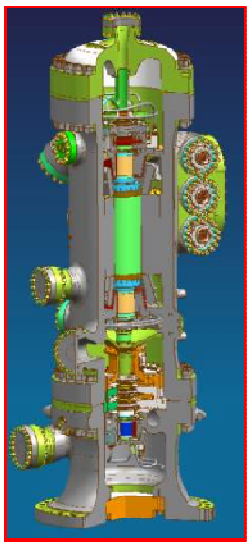

Figure 2 – Motorcompressor 3D view.

The unit is quite compact with respect to the power rating: 6m (19.7ft) in height and 2m (6.6ft) in diameter, with an overall weight of 55t (121254lb) (not including the external seawater cooler).

The three-journal bearing rotor was considered a very robust solution for smooth rotordynamics associated with a high rotational speed. In fact, three rotor modes are crossed in this configuration but they are all critically damped. This is made possible also thanks to the AMBs, which take advantage of the absence of the gravity load, saving load capacity for the lateral dynamics. For reference the AMBs are named #1, #2, #3 going from the top to the bottom (e.g. AMB#3 is the compressor bearing).

The axial magnetic bearing is located on the top and is of the double effect type, since the global axial load can be reversed during operation.

The AMBs are all canned, which means that the statoric parts are completely enveloped with stainless steel protective cans. This technology was qualified during the project and the authors believe it is a big plus for the subsea compression application.

On the electric motor side, state-of-the-art technology in terms of high speed, process cooled motors was used. The motor was integrated in the motocompressor environment and made as robust as possible and insensitive to potential process upset conditions. For instance, the cooling gas is filtered and then maintained in a closed loop, the casing material is made of stainless steel to avoid rust and deposits on the magnetized parts, and the layout is vertical to allow drainage of liquids.

The unit allows for the collection of liquid slugs on the bottom sump that is sized for 500l (132.1gallon).

The compressor is conceived as a cartridge, which can be removed from the electric motor section if a rebundle is needed. The maximum number of impellers is dictated by the available room in the suction plenum and also by a compromise with the rotordynamic behaviour. The compression service for the current application is fulfilled with a three-wheel rotor. Finally, this solution is fully marinized and ready for submerged testing.

FULL LOAD TEST DESCRIPTION AND RESULTS

Test program

The motorcompressor test bench was erected at the Authors' Company facility at Le Creusot (see Figure 3) and the test started in January 2010. The test was intended as a general functional qualification test for the motorcompressor preliminary to the validation phase at the costumer's site (submerged test).

The test program consisted of the following main steps:

- Tuning of the AMBs
- Mechanical Running Test
- Compressor Performance Test
    - Similitude (ASME PTC-10 Type II)
    - Maximum load test (10MW vs. 12.5MW)
- Overall cooling system check
- Landing test
    - Partial landing
    - Full speed landing

All these steps contributed to the overall motorcompressor validation in terms of:

- Compressor Thermodynamics
- General Rotordynamics
- System Cooling
- Axial Thrust
- Electric Motor
- AMB Control System
- Full speed emergency landing

Since the test data were critical to the validation of this technology, the instrumentation setup was of special importance and is described in detail below.

Figure 3 – Le Creusot test bench.

Instrumentation

Dedicated instrumentation was installed on the machine and test facility in order to validate the new design, to data-match analytical models and to monitor test parameters.

The areas of primary interest in the validation testing were:

- System cooling
- Auxiliary bearings
- VSDS Electric-Network and Motor Power Analysis
- AMBs

The data acquisition system was designed to act as a single entry point collecting data coming not only from special instrumentation, but also from the test rig control panel and AMB cabinet.

System cooling (Motor and bearing cooling)

System cooling in the subsea motorcompressor is designed to provide cooling flow to the AMBs and to the electric motor. The system is composed of a quasi-closed loop for the cooling of motor-side devices and an open loop for the compressor-side bearing and seal buffering (see System Cooling paragraph for more details).

The scope of the measurements is to provide data (pressure and temperature measurements) for validation of the secondary flows (cooling flows) model.

For pressure measurements, miniature piezo-resistive high-pressure transducers were installed inside the machine. This solution, requiring minor machining, was preferred to traditional pneumatic measurements, both because of reduced intrusion and increased intrinsic safety.

Temperatures were measured with RTDs; in low accessibility areas, pressure sensors were equipped with onboard Pt1000.

Wiring was routed through dedicated flanges on the casing. In order to minimize the risk of leak, high pressure, high-density conductor sealing glands were selected. This type of gland assembly, due to its insulated, compact, uninterrupted copper wires, guarantees physical disconnection and no leakage through wire protection in case of sensor failure. The design of the installation, including external routing in the test facility area, is compliant with the applicable EC Directives.

Auxiliary Bearings

Vibration monitoring of auxiliary bearing housings was performed during landing test execution to check (on-line) the vibration level reached, as a follow up of previous laboratory tests (Ransom et al., 2009). Miniaturized 3-axial accelerometers ICP with integrated cable were screwed onto the auxiliary bearing housings. Additionally, the overall machine casing vibration monitoring during landing tests was done using ATEX compliant mono-axial accelerometers installed on the top flange of the motorcompressor body.

VSDS, Electric Network Grid and Motor Power Analysis

VSDS components were instrumented in order to data-match the analytical model and to perform power analysis.

Network power analysis: Dedicated voltage and current probes were placed on the main transformer bus-bars (inside the power cabinet) and were measured using a power-meter with Harmonic Analyzer capability.

VSDS output filter temperatures were measured by PT100 type RTDs installed on the filter coils, measured by a dedicated data logger placed on site.

Due to the distance between the Control Room and the Frequency Converter/Main Transformer location, the static and dynamic acquisition system had to be doubled and localized: connection with the control room was realized through a dedicated fiber optic link.

Motor power analysis: voltage and current probes were installed on the intermediate junction box located close to the motorcompressor. In order to correctly measure all harmonics up to the 50th, all the probes selected had a high bandwidth.

During an extensive front-end calibration campaign performed on site by the metrology lab, in particular, the frequency response of voltage probes was shown to be strongly affected by the cabling length and acquisition conditioning. The result of the optimization was a set of HV probes with an internally compensated integrated 30m (98.4ft) extension cable designed to compensate stray capacitance, and custom tuned conditioning boards: the accuracy was within 1% of the reading up to 8.5kHz.

All data, including those retrieved from the Test Control Panel (such as data from the VFD and compressor performance) were collected and recorded. Visual panels (see Figure 4) were used during running to perform checks on the system functionality.

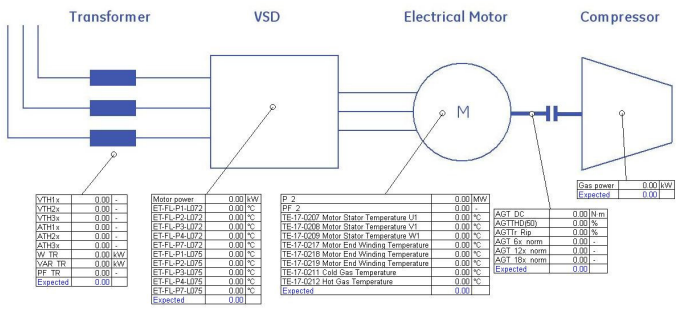

Figure 4 –Visual panel for motor performance evaluation.

AMBs

Operating parameters from the AMBs (currents, coil temperatures, displacements) were recorded and synchronized with the rest of data.

When possible, physical connections to the AMB control cabinet were used for direct high-sample-rate acquisition: this was possible for speed, axes positions and currents.

As for other slowly varying signals, such as bearing temperatures, they were indirectly retrieved from the test control panel via Ethernet. The connection between the UCP and AMB cabinet was via MODBUS protocol.

Overall, the integrated acquisition system (see Figure 5) was highly beneficial, allowing the synchronized acquisition of all data coming from both the test facility and the machine. This made it possible to perform system-level analyses, with direct comparison between different system component trend-lines, making the identification of cause-effects relationships easier and simplifying troubleshooting.

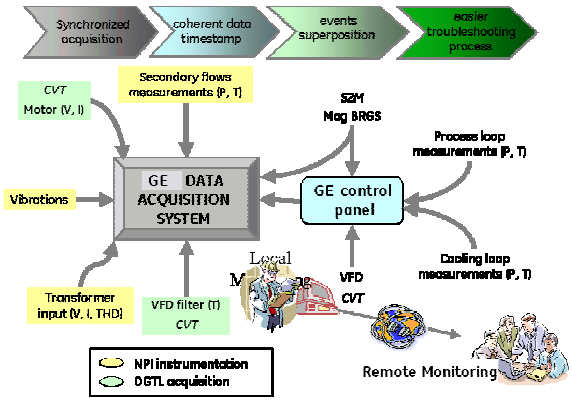

Figure 5 – Integrated acquisition system.

Compressor Thermodynamics

Initially, the performance test was executed at low pressure according to the similitude criteria of ASME PTC-10 code and later at full pressure to match the site conditions. It is important to note that the compressor duty is based on many operating points, which represent the evolution of the gas reservoir life. The delivery pressure is always constant at 140bar (2031psi) while the suction pressure decreases more and more over the time: the starting suction pressure is just below 140bar and the target final plateau value is 80bar (1160.3psi). This means the compressor starts to operate at its minimum rotational speed and increase the speed along the years. For this reason the motorcompressor operating range is very broad with a minimum operating speed (mos) of 3048rpm and a Maximum Continuous Speed (MCS) of 10668rpm.

The compressor performance was in general agreement with expectations. Figure 6 shows the result of the low pressure performance test conducted at 25bar (362.6psi) in terms of the non dimensional parameters psi and eta with respect to the flow coefficient.

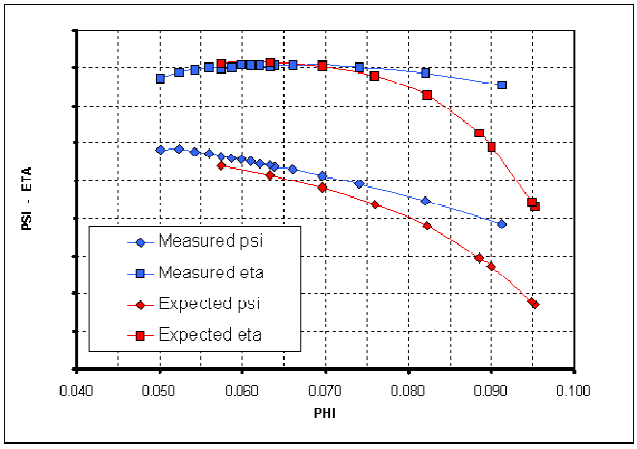

Figure 6 – Expected vs. Tested compressor performances.

The efficiency is generally flat and higher than expected at high flow while it is in line with or slightly below expectations at low flow. The head is always higher than expected. During the low pressure test, the surge region of the compressor was explored in order to find the operating limit: the operating point was extended up to 14% less flow than the expected right limit without any evidence of surge.

General Rotordynamics

Special consideration to rotordynamics and AMB performance was given during motorcompressor testing to validate the predictions and assess the robustness of operation at different operating conditions.

Due to the lack of specific design and acceptance test requirements in the API617 Standard for integrated motor-compressors equipped with AMBs, ISO 14839-2/3 Standards acceptance test requirements in terms of vibration amplitude and stability performance were applied, with the concurrence of the customer. Aiming to target the most conservative acceptance values for newly commissioned machines, in the Zone-A class of merit, the following ISO 14839 criteria were selected:

- Maximum allowable rotor displacement (0-Pk), equal to 0.3 C_{min} (where C_{min}=200µm / 7.88mils) is the minimum radial clearance inside the machine and corresponds to the auxiliary bearing air gap).
- Maximum allowable Peak Sensitivity Transfer Function gain ($|G_s|$) equal to 3 (9.5 dB).

To target these requirements, an extensive rotor and AMB system design and optimization (requiring extension of both Authors' Company and AMB Supplier tools and design criteria) was carried out during the development phase, as explained in Masala et al., 2010. The objective of targeting ISO 14839 requirements was made even more challenging due to the following specific features and technical innovations introduced in this prototype:

- A rotor configuration supported by three AMBs and with one honeycomb seal on the balance drum,
- The presence of the canning on the AMBs, affecting the dynamic performances and introducing possible gas induced aerodynamic cross-coupling excitation.
- The machine vertical configuration, which required an integration of the rotor and AMB dynamics with the casing and overall structure dynamics.

The rotordynamic performance validation was carried out in three major steps:

I. AMB control system tuning
II. Mechanical running test
III. Performance test

The first task was required to validate the predicted rotor and AMB transfer function, as determined during the design phase, and to identify the proper control parameters to provide suitable stiffness and damping over the AMB controller bandwidth. In this regard, it was of special interest to identify:

- The actual position of the 1st rotor bending mode, which was within the operating speed range of the machine and required proper AMB controller parameter to be critically damped.
- The actual position 2nd rotor bending mode, which was above the maximum continuous speed and had by a low damping ratio, requiring suitable separation margin from MCS.
- All high frequency dynamics of the rotor and correct interlacing violations generated by sensor and actuator non-collocation, as already addressed during the design phase, and deviation of the AMB system dynamics from predicted

model.

The rotor system identification revealed good correspondence of the 1st bending mode of the rotor with the calculated value, whereas some deviation on the 2nd and 3rd bending mode was identified, as depicted in Figure 7.

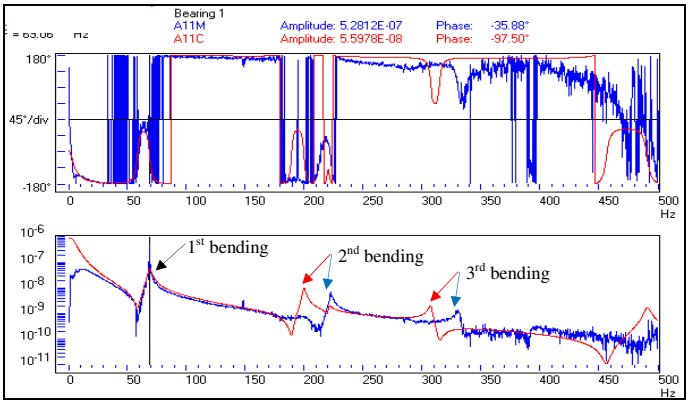

Figure 7 - Rotor transfer function check. Measured (blue) and predicted (red) rotor response.

The potential deviation of the actual rotor bending modes from predicted values had already been identified during the rotor free-free test performed at Authors' Company plant, prior to installing the rotor in the machine. Since the deviation was in the conservative direction, as the actual separation margin of the 2nd bending mode from the operating speed range was higher compared to the predicted value, the modification of the control system was deferred to the tuning phase.

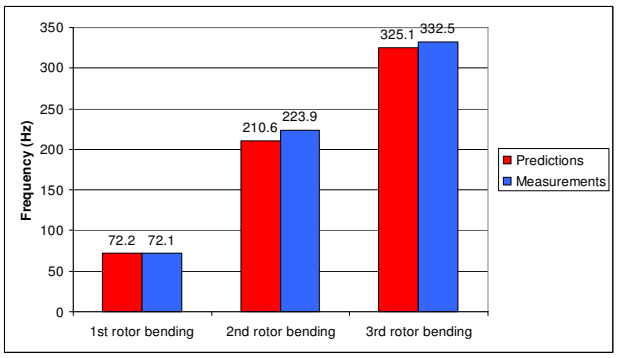

Figure 8 - Calculated and measured free-free bending modes.

Another important task addressed during the tuning phase, was to identify proper rotor centering inside the auxiliary bearing air gap. Because of installation tolerances between the auxiliary bearings and the magnetic actuator, proper identification of the reference center of rotation, with respect to the ideal position, is required for any AMB supported rotor. In this case, the task was even more challenging because the rigid rotor was supported by three AMBs and some amount of mounting misalignment was present among them, despite the tight manufacturing and installation tolerances. The centering procedure was performed, for each AMB, as a trade-off between the minimum rotor deflection (involving a consumption of AMBs load capacity), and the best geometrical rotor centering in the auxiliary bearing air gap.

The AMB tuning procedure performed at stand-still condition was finalized as the machine started to run and the speed increased up to maximum continuous speed. A step-by-step speed increase was setup to verify the correct controller parameters and arrange the settings of the synchronous filters to cross the critical speed inside the operating speed range while reducing the vibration amplitudes.

The final settings of the AMB controller parameters allowed reaching the maximum continuous speed during mechanical running test with very smooth crossing of the critical speeds and low vibration amplitude, with the synchronous filters either activated or deactivated, as depicted in Figure 10 and Figure 11.

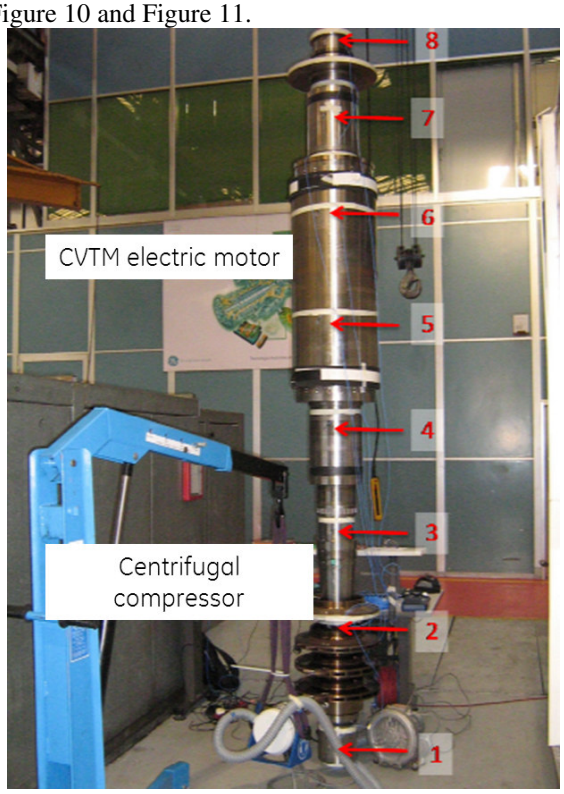

Figure 9 - Rotor free-free test.

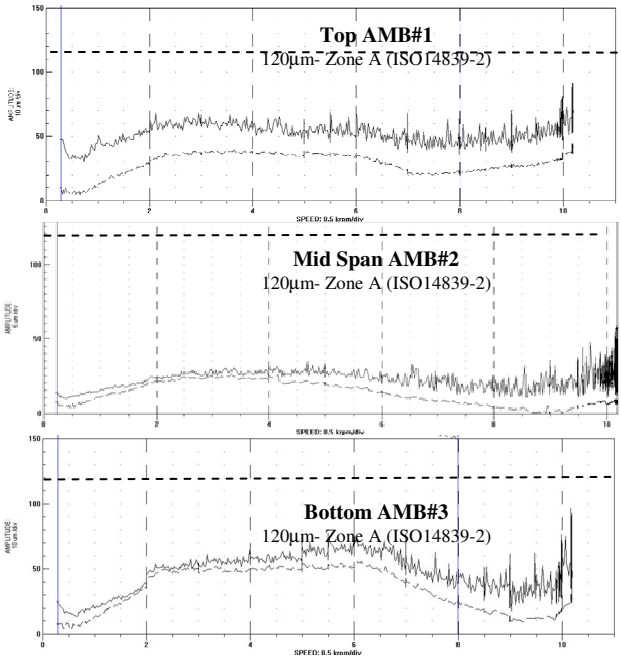

Figure 10 - Rotor vibration amplitude (1µm=0.04mils) on AMB#1, AMB#2 and AMB#3 with Synchronous Filters deactivated.

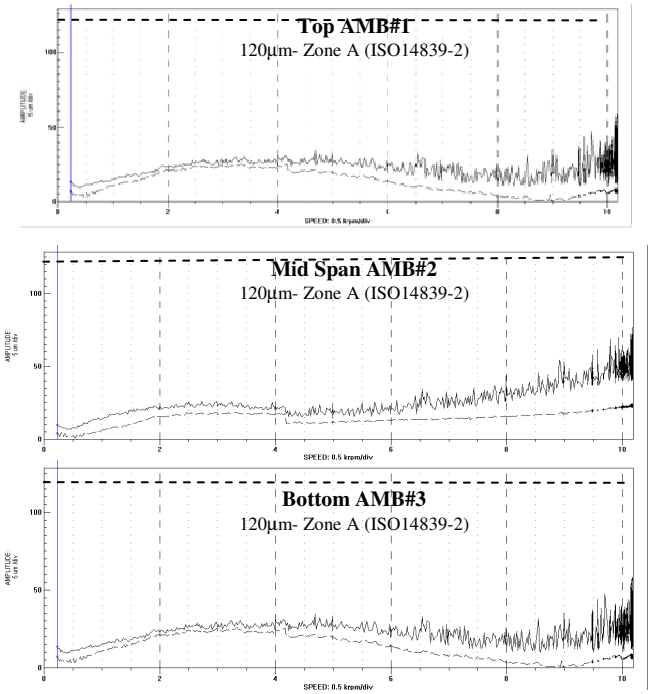

Figure 11 - Rotor vibration amplitude (1µm=0.04mils) on AMB#1, AMB#2 and AMB#3 with Synchronous Filters activated.

A further control system adjustment was required during the machine performance test to limit the vibration amplitude in the low and high frequency range as different operating points on the performance map were explored.

Due to reduced AMB stiffness in the 10÷70 Hz frequency range, AMB-equipped machines are susceptible to low frequency broadband excitation induced by fluid and aerodynamic instabilities, which increase with the gas power delivered by the machine. During motorcompressor testing an odd sub-synchronous vibration, tracking the rotor speed with a ratio of approximately 1:6, was identified when the machine was operating with higher pressure and speed. Surprisingly, the sub-synchronous vibration was not fixed in frequency, hence not correlated to rotor mode excitation, neither correlated to gas flow rate and pressure ratio, which excluded the possible correlation of the phenomena with fluid instability on compressor impellers or stationary parts.

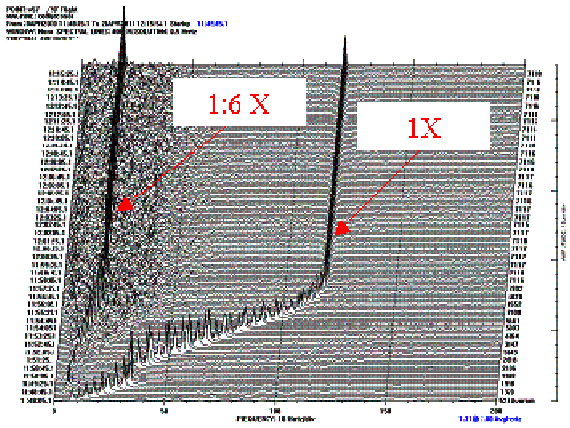

Figure 12 - Sub-synchronous vibration (1µm=0.04mils) tracking rotor speed.

While operating on the AMB cooling flow system to test the effect of the cooling gas flow rate on AMB temperature, it was found that as the flow on mid-span AMB2 was increased by opening the valve on the injection line, the sub-synchronous vibration suddenly disappeared, as depicted in Figure 12.The correlation with the cooling gas injection provided an important clue on the source of the excitation, which was corrected by changing AMB2 cooling path and fan geometry. Overall, the experience was an important observation on how closely related the phenomena are in integrated machines, and how secondary flows can impact the machine dynamic performance.

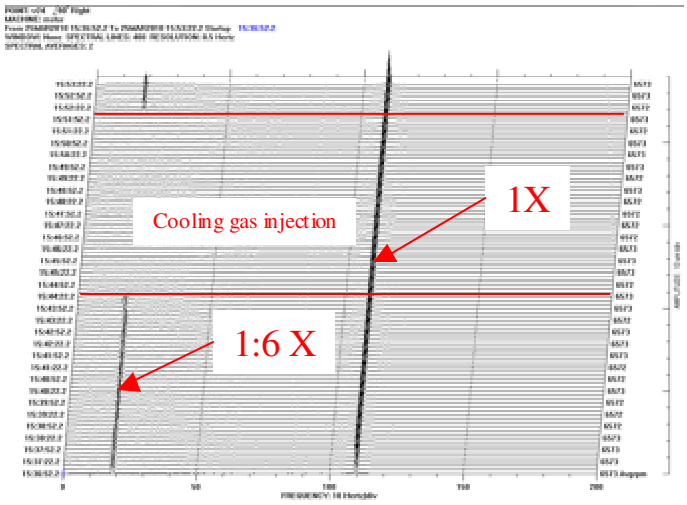

Figure 13 - Subsynchronous vibration (1µm=0.04mils) suppressed by injection of cooling flow on AMB2.

From a stability standpoint, the stability check based on the peak sensitivity transfer function, combined with AMB Supplier internal stability criteria, confirmed good stability margin, in accordance with ISO14839-3 requirements and predicted values, as depicted in Figure 14.

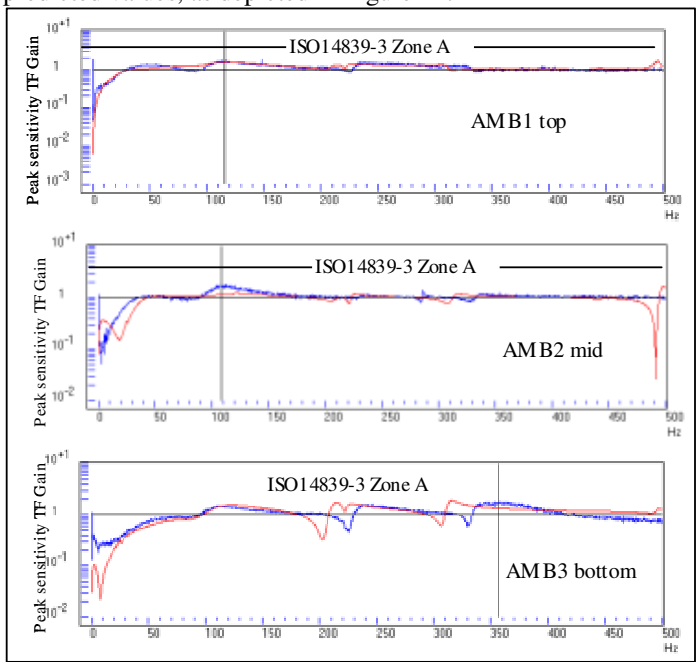

Figure 14 - Stability check according ISO14839-3 on AMB1 (top), AMB (mid-span), AMB3 (bottom) – Measured (blue) and predicted (red) Peak Sensitivity Transfer Function.

System Cooling

The cooling of the motorcompressor system was completely new since it was designed for the purpose of this new configuration (see Figure 15). Since the cooling medium is the process gas, a special attention was paid to protect the electric motor and the AMBs. Regarding the AMBs, they were protected through the canned design, which isolates the stator coils from any contaminant present in the cooling gas. The electric motor, on the contrary, is based on more standard technology with stator parts directly exposed to the gas. For this reason, special care was given by the manufacturer to increase the coil insulation thickness and to increase the robustness towards liquids. In any case, the cooling network was designed to keep the electric motor volume in a controlled environment, separate from the process. In fact, the motor cooling flow, driven by a small fan installed on the motor shaft end, passes through respectively the AMB#1, the motor stator and air gap, AMB#2 and finally is routed out the casing towards an external cooler. This is basically a closed loop where the gas is the process gas but is provided only once for all at the startup of the motorcompressor from the compressor after a filtering stage (clean and dry gas).

Instead, the compressor bearing cooling is from a flow, which is extracted from the compressor flow path after a double filtering stage.

Finally, a buffer line is provided between the electric motor and the centrifugal compressor to seal the motor environment and keep it clean.

The system cooling was verified during FAT both at partial and full load.

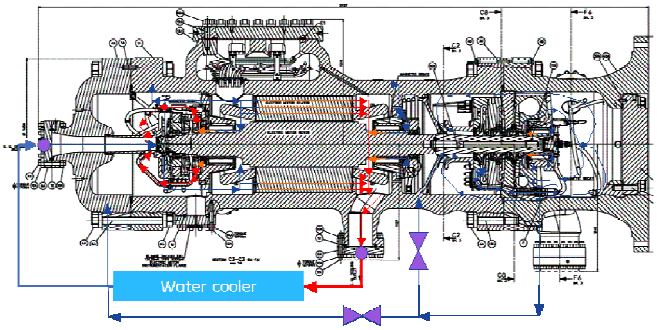

Figure 15 – System cooling: overall network.

The results of two different runs are shown in the figures below. Figure 16 and Figure 17 show the AMB coil temperatures and the EM stator temperatures relevant to the full load test.

Figure 18 and Figure 19 show the same temperatures for a minimum pressure case with the motorcompressor running at MCS.

It is worthwhile to mention that both the AMBs and the EM show critical conditions from a thermal point of view in the following scenarios:

- Minimum pressure and maximum speed
- Full load

The AMBs are mainly heated by the windage losses in the air gap (which are dependent especially on the rotational speed) but the available cooling mass flow is lower when the pressure is at the minimum level. Moreover, the EM shows lower electrical losses when the pressure (hence the compressor load) is at a minimum level but the point of the lower cooling mass flow at minimum pressure holds true as well. So both the operating conditions were checked as described below.

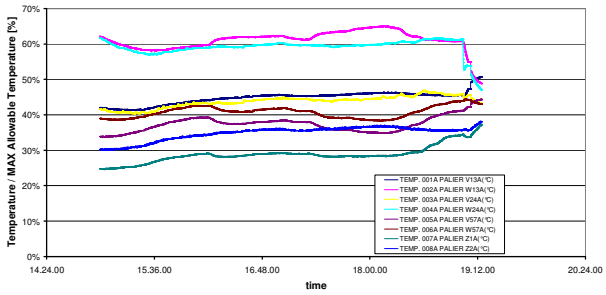

Figure 16 –Temperature of AMBs from full load test.

The main outcome of the FAT was the demonstration of the cooling system full functionality at full load and the verification of the minimum pressure achievable. In further detail:

- The AMBs were operating below 70% maximum allowable temperature at full load and below 95% at 45bar (652.7psi) (minimum pressure).
- The EM stator was operating below 60% maximum allowable temperature at full load test points and below 65% at 45bar (minimum pressure).

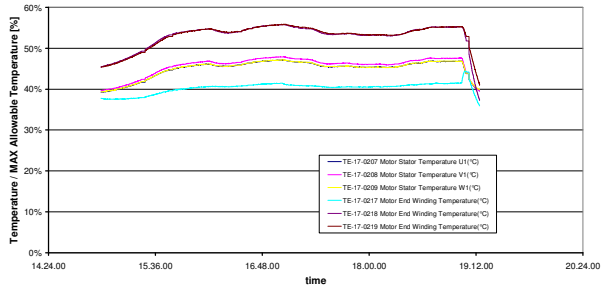

Figure 17 – EM temperatures from full load test.

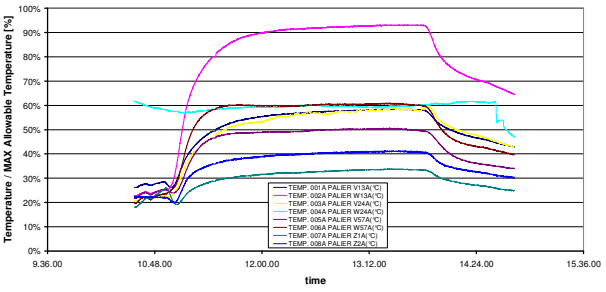

Figure 18 – AMB temperatures from minimum pressure test.

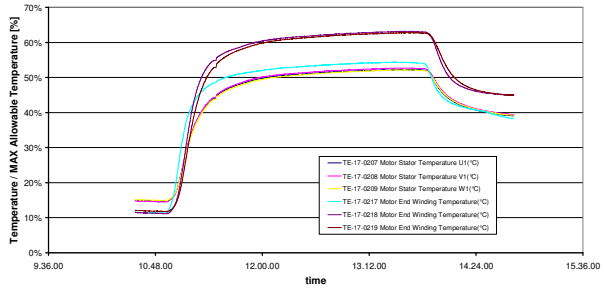

Figure 19 – EM stator temperatures from minimum pressure test.

The separation system which is implemented in the compressor is also valid for the liquid phase and this feature can be applied for wet gas conditions. In order to demonstrate this specific capability a dedicated validation testing has been performed in a dedicated external rig built at Southwest Research Institute in 2010.

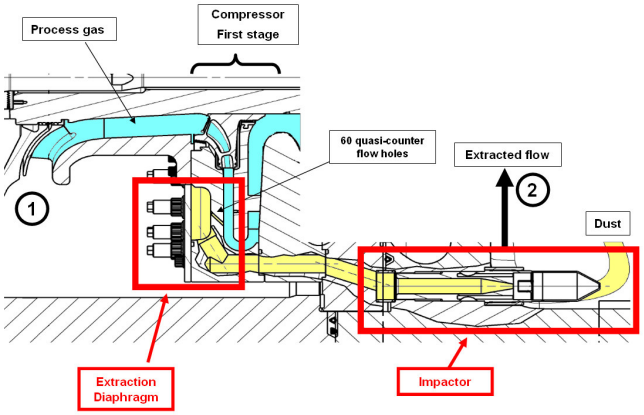

Figure 20 - Extraction system layout.

The extraction system (see Figure 20) is composed of an *extraction diaphragm*, which separates the cooling flow from the first stage diffuser by means of 60 quasi-counter flow holes, acting as a primary separator and an *impactor* acting as a secondary separator.

The wet gas tests were performed on a two-stage centrifugal compressor working with air-water mixtures and equipped with an equivalent separation system. The test conditions were as follows:

- Suction pressure: 20bara
- Liquid volume fractions (LVF): 0.3 ÷ 5% (up to 72% in liquid mass fraction)

$$LVF = \frac{\dot{Q}_{l,1}}{\dot{Q}_{g,1} + \dot{Q}_{l,1}} \qquad (1)$$

In order for the test to be representative of the real machine, the same design criteria were used to size the separation system of the test compressor. The impactor was geometrically scaled down to 67% of the original one to keep the same nozzle Mach number, while the diameter of the extraction holes and the test conditions were chosen to match the Stokes number.

The separation efficiency for both the diaphragm and the impactor was measured and finally, the overall system efficiency was calculated and is shown in Figure 21. The overall system efficiency is defined as:

$$\eta = 1 - \frac{\dot{Q}_{l,2}}{\dot{Q}_{l,1}} \qquad (2)$$

where $\dot{Q}_{l,2}$ is the liquid flow rate of the extracted secondary flow and $\dot{Q}_{l,1}$ is the liquid flow rate of the compressor process gas.

The test results show that the separation efficiency of the extraction system is close to the typical value of high efficiency separators: it ranges from 98.65 to 99.45% without any net dependence on LVF.

These tests demonstrate excellent separation performance under wet gas operation.

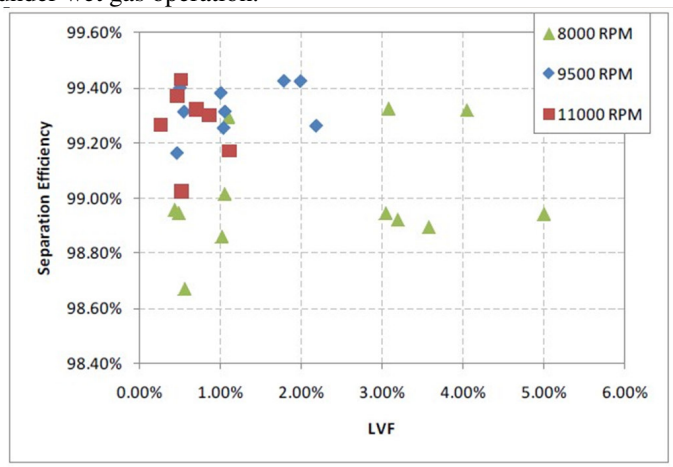

Figure 21 - Extraction system separation efficiency versus LVF.

Axial Load

In order to evaluate the axial load for this motorcompressor it is necessary to analyze all the contributions along both the electric motor and the centrifugal compressor rotor.
For this purpose a model was developed, which is represented in Figure 22.

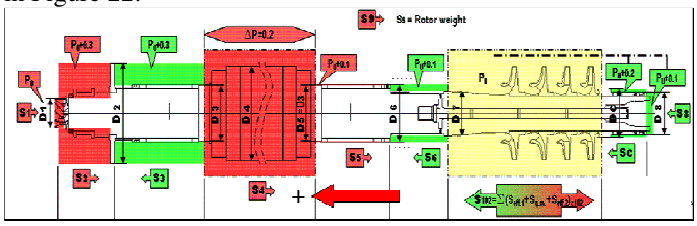

Figure 22 – Axial load model.

The sign convention should be noted: a positive axial load means the rotor is pushed to the top.

The contributions to the axial load are given by the following effects (including the direction):

- All static pressures insisting on the rotor surfaces: load direction depends on surface position
- Centrifugal compressor primary effects (static pressure across the stages): positive load
- Centrifugal compressor axial momentum change: negative load
- Centrifugal compressor secondary effects (pressure distribution in the compressor cavities): positive load
- Balance piston: negative load

The axial load predicted curves versus the compressor flow are shown in Figure 23.

During the test, a general mismatch between the predictions and the measurements was noticed, with the measured axial loads greater in the downward direction (negative sign according to the sign convention). The measurement of the axial load was possible through the currents of the axial magnetic bearing.

This gap made it difficult to operate the compressor in the high flow region where the load is mainly downwards due to the high axial momentum in the compressor section. In fact, during the test when the compressor operating envelope was

mapped, the last stable point on the right was reached due to the saturation of the axial load capacity.

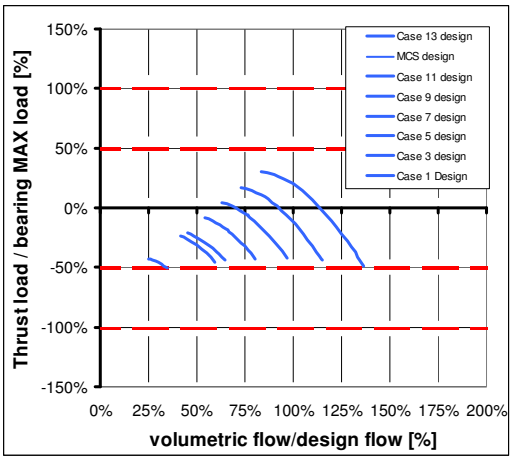

Figure 23 – Axial load predicted curves.

In order to enlarge the operating range at high flow, a trimming of the balance piston was finally performed leading to a 6% gain in the maximum flow that could be handled. Figure 24 shows the predicted compressor envelope (defined by the continuous curves) and the associated test points. It is easy to see that the compressor was working properly on the operating points (white circles); while in the high flow region the last point corresponded to a limit in the axial load. The red line was the original limit while the green line is the final limit after trimming the balance piston.

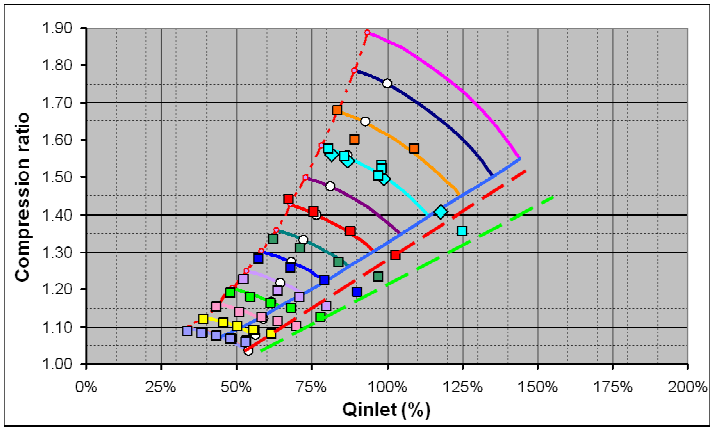

Figure 24 – Compressor operating envelope.

The lesson learned from this test is that the axial load is a critical parameter for this type of machinery and the predictability of the axial load is even more complicated than for traditional centrifugal compressors due to the presence of the rest of the system. Moreover, the lower load capability of the AMB with respect to a hydrodynamic bearing requires the axial load estimation to be performed with a higher level of accuracy. An uncertainty analysis on the key parameters affecting the axial load (especially the pressure distribution across the entire rotor) is needed for a more robust design.

Electric Motor

At the Le Creusot site the available Frequency Converter was a drive from the MV7000 family (12MW @ 50Hz). Due to the limitation of the drive, the maximum shaft power achievable at 170Hz during the string test was 9.8MW (12740HP).

A dedicated sinus filter was installed in the output of the VFD in order to reduce the harmonic content to the motor, thus preserving the motor insulation. The sinus filter was water-cooled.

The motor was connected to the drive basically with 300m (984ft) of power cables of the following sizes: one section with 3 x 400mm^2 (0.62in^2) per phase and another one of approximately 100m (328ft) with 4 x 240mm^2 (0.37in^2) per phase.

Discharge resistors (3MJ / 1.12HP-h) were installed in the output of the sinus filter with the aim of reducing self-excitation phenomena. The self-excitation is generated by the resonance between the filter, power cable system and motor when an emergency trip is commanded to the VFD (in this case, the output inverter stop to pulse). The discharge resistors are activated by a Ross Relay (with a release time of 80ms).

The electrical power connection in the motor-compressor is done through a pass-through. This system replaced the job high voltage connectors that were not suitable for connection to the shop cabling.

On the motor side, the pass-through is connected to one of the three flanges of the motor junction box (all 12 motor power cables are carried out from this flange) and is able to withstand the differential pressure between the motor room and the external environment. On the other side, the cabling is connected through about 3m (9.84ft) of piping to an external junction box. The picture below shows the motor-compressor with the pass-through system and the JB.

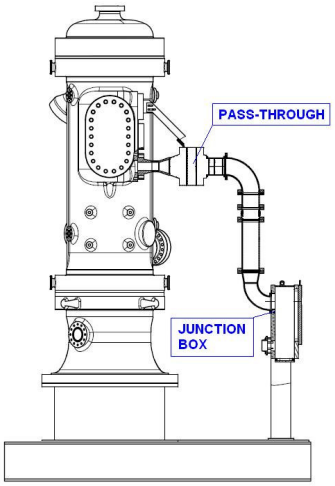

Figure 25 – Motor-compressor with pass-through

All motor instrumentation (voltage and current probes) was installed in the junction box.

The motorcompressor was tested under 11 cases (over the 13 contractual operating points), each one at fixed speed; several points were taken for each case (changing the compressor gas flow) in order to build the compressor curves. For each point the whole system was monitored and all data were recorded. In this section, the measurement and results related to the motor are presented. The relevant points from the 11 cases are shown in Table 1.

The power input to the motor were calculated from the voltages and currents measured at the motor terminals. The motor active power at the terminals is calculated according the following formula:

$$P_{MOTOR} = \frac{1}{T}\int_T (v_{f1}\cdot i_1 + v_{f2}\cdot i_2 + v_{f3}\cdot i_3) \quad (3)$$

where v_{f1}, v_{f2} and v_{f3} are the phase-to-ground voltages. The Authors' Company acquisition system performed these calculations in real time.

	Frequency [Hz]	Pressure [barg]
1	63	135
2	73	130
3	82	125
4	91	120
5	99	114
6	109	109
7	119	105
8	128	99
9	148	88
10	154	85
11	178	45
12	146	88

Table 1 – Pressure (1barg= 14.5psig) and speed of the main test points.

The Power Factor is calculated according to its definition:

$$p.f. = \frac{P_{MOTOR}}{S} \quad (4)$$

where S is the Apparent Power.

The electric motor performance was evaluated comparing the losses in the motor with the difference between the motor (input) power and the process gas power, and with the heat dissipated in the external cooler.

The expected losses in the motor come form the calculations performed during the engineering phase; basically, the comparison between the motor losses with the test measurements provides the estimate of the motor performance.

The motor losses are the sum of the following three values:

- Iron losses: losses in the iron of the stator, directly proportional to the voltage at the terminals.
- Copper losses: losses in the copper due to the currents.
- Windage: losses induced by the windage of the gas due to the high speed of the rotor.
- DeltaP: the difference between the motor power at the terminals and the power delivered to the process gas.

$$DeltaP = P_{MOTOR} - P_{GAS} \quad (5)$$

The heat dissipated in the external cooler is calculated with the following formula:

$$\Delta\dot{Q} = H_{SP}\cdot\dot{m}\cdot\Delta T \quad (6)$$

where H_{SP} is the gas specific heat based on the Authors' Company real gas database and ΔT is the difference between the hot gas temperature (input to the cooler) and the cold gas temperature (output from the cooler).

The main results are presented below. Figure 26 shows a comparison between the expected efficiency and the measured efficiency.

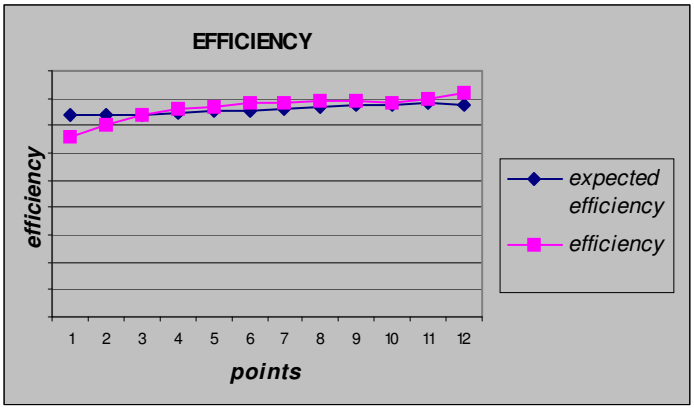

Figure 26 – Electric Motor efficiency evaluation.

Figure 27 below shows a comparison between the expected power factor and the tested power factor.

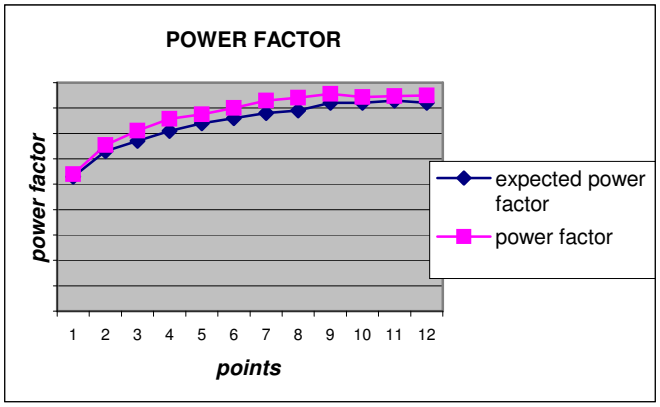

Figure 27 – Power Factor evaluation.

Figure 28 shows a comparison between the losses from the calculation done during the engineering phase and the losses calculated from the real data measured.

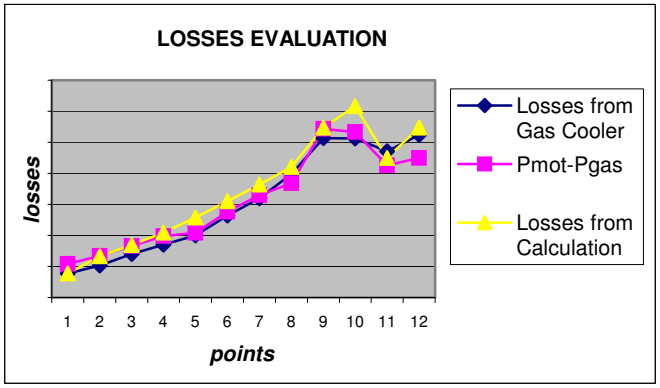

Figure 28 – Comparison between the DeltaP, the losses in the cooler and the Losses from the calculation.

Basically two main conclusions come from the test:

- The electric motor showed good performance in terms of both efficiency (above 89% from point 6 [6600rpm, 110bar/1595psi, 4.5MW/6035HP shaft power]) and power factor (0.84 from point 8 [7700rpm, 100bar/1450psi, 6350KW/8516HP]).
- The electric motor showed very good predictability: in all cases, the calculated losses are

comparable to the values measured in the field (in some cases the performance is even better than predicted).

AMB control system

Because of the peculiarity of the environment and the machine the project required the development a completely new AMB control system; an architecture based on redundancy of the main devices was defined in order to satisfy the reliability and availability requirements. The 7-axis control loop is implemented through a Digital Signal Processor at 13.8KHz, while the power electronics are based on the supplier's standard 300/30 (300 volt / 30 A).

The reason for a 7-axis control system is that the machine is equipped with three radial and one axial bearing (totaling 7 axes: 2 X 3 radial bearings and 1 X 1 axial bearing). Until now a 5 + 5-axis control system has been used for this type of application.

An internal Profinet network, a sort of real-time Ethernet communication protocol, guarantees the high throughput data exchange between the devices that are managing the raw data and the MBCSI (Magnetic Bearing Control System Interface), which is collecting all data and transferring it to the topside station.

The AMB control system is divided into two main parts:

- embedded control system, which will be installed in the subsea environment
- remote control system; which will be installed in the control room

The embedded part is an assembly of electronic devices that are mainly used to implement the control loop, protection of the machine and the interface to the remote systems.

The remote part, based on an industrial PC and dedicated software, is used specifically for the remote tuning of the machine and remote monitoring that continuously collects and stores the data analyzed by the embedded system; the stored data can be post-processed and used for diagnostic purposes.

The control system was developed in the AMBs Supplier laboratories where it was validated through a scaled down model of the machine rotor. The control system functionalities were validated through extensive integration test sessions.

The string test was conducted with an industrial version of the AMB control system for practical reasons since the marinized version was still being qualified in a rigorous program for that purpose. Nevertheless, both versions are equipped with the same electronic devices and so the same functionalities are guaranteed.

One of the most important features of the AMB control system is the ability to be controlled and configured from a remote control station using a network connection. A specific tool was developed by AMBs Supplier for this purpose.

A dedicated session was organized for the validation of the remote tuning tool. The test consisted of a comparison between the measurements (open loop, closed loop, and sensitivity transfer function) done using a commercial spectrum analyzer and the measurements performed with the digital spectrum analyzer tool included in the software suite. This tool will be used when the machine is installed subsea (on the seabed or in the test pit) and the control system will be no longer be accessible with traditional equipments. This test demonstrated that it is now possible to evaluate the rotordynamic behavior of the system and to tailor the control loop parameters for the motorcompressor using a remote station connected to the AMB control system only through a network connection.

Full speed emergency landing

The final step of the FAT consisted of the rotor drop test onto auxiliary bearings to prove the required tolerance of the unit to unexpected rotor delevitation events that might occur during the machine service life. Because of the extreme importance of this feature for motorcompressor units installed on the seabed and the requirement for very limited maintenance, five drops from full speed condition down to standstill were planned, as agreed by the AMB vendor, the OEM and the final customer. The five drop test sequence, which by far exceeded typical API617, 7th ed. 2001, requirements for turboexpanders [ref. Annex 4F] (generally limited to two delevitation events and for a limited interval of three seconds), was the most challenging and risky aspect f the entire FAT.

For this test, the past experience on a scaled test rig for a vertical rotor drop onto auxiliary bearings (Masala et. al, 2009) and the results of the simulation performed to predict the landing dynamics of the full scale machine, were leveraged and incorporated into a drop test procedure. Starting from the primary goal to protect the integrity of the machine, Go/No-Go criteria were identified to decide, whether to proceed to the next planned drop sequence or not after each drop.

Some indicators of auxiliary bearing failure had successfully been identified during the endurance test performed at the SwRI laboratories on the scaled test rig, as reported in Masala et al., 2009). Since it was not possible to determine the failure threshold level for the full-scale machine from past experiments, the Go/No-Go criteria were based on the deviation of the measured parameters from the 1st drop of the sequence performed during the FAT. The following parameters were compared to the 1st drop measured values and corresponding limits:

- Rotor vibration amplitudes at sensor location and whirl frequency (Ω)
- Rotor deceleration rate from 2000 rpm to minimum speed
- Vibration signature of auxiliary bearings supports
- AMB and rotor transfer function
- Clearance checks of auxiliary bearings
- Machine performance checks

The check of the rotor whirl amplitude was aimed at verifying that the rotor orbit was lower than 75% of the minimum clearance values inside the machine and excluding the possibility of rotor rubbing at the AMBs and seals. In addition, the combination of the whirl frequency and amplitude, together with the mass of the rotor, were used to determine a conservative value of the loads exerted on the auxiliary bearings and to compare this value to the corresponding allowable level.

The remaining parameters, i.e., the deceleration rate, the vibration signature, the rotor transfer function, the auxiliary

bearing checks and machine performance, were used on a comparative basis to identify possible performance degradation or damage of the auxiliary bearing and rotor system. To be able to compare the mentioned parameters after each drop, all five of the drops had to be performed from the same rotor drop condition. This condition was selected as a reasonable operating point of the machine running at full speed, with suitable separation from the surge line to prevent the compressor from surging during the transient delevitation. The selected drop conditions are summarized below:

- Rotor Speed, ω = 10160 rpm
- Gas Suction Pressure = 64 barg (934psig)
- Gas Discharge Pressure = 106 barg (1532psig)

Prior to starting the real drop sequence, a rotor trip simulation and a rotor re-levitation check were performed.

The trip simulation, performed from the selected drop conditions, was aimed at assuring that the required separation margin from the surge line was guaranteed during coast-down and that the deceleration rate of the machine was comparable to the forecast level. Both conditions were successfully verified during this test. In addition, the measurements of the currents on the axial AMB coils, collected during rotor coast-down, provided some important tips on the transient of the resultant loads exerted on the rotor during the drop sequence, unveiling an unaccounted axial load inversion due to modification of the pressure pattern profile across the rotor as the machine speed was decreasing.

The re-levitation test, performed at rotor speed of 2000 rpm, confirmed the capability of the AMB control system to regain control of the rotor position after a few seconds of delevitation. In addition, the rotor orbit clipping identified during this test, as depicted in Figure 30, provided an important clue about the necessity to modify the nominal sensor settings of the AMBs, which were typically set to measure the limited rotor orbit during normal operation of the AMBs, to be able to detect the full orbit during the rotor drop. With the modified sensor settings, a larger measurement range was gained.

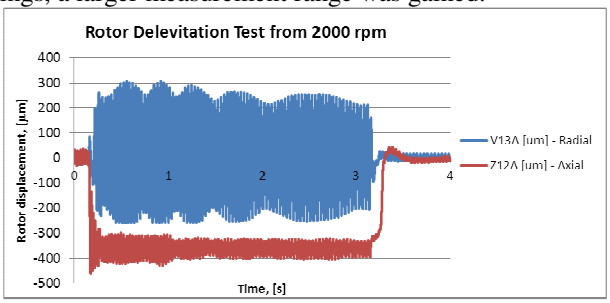

Figure 29 - Positions (1µm=0.04mils) on the 1st bearing (blue) and axial bearing (red) during partial landing.

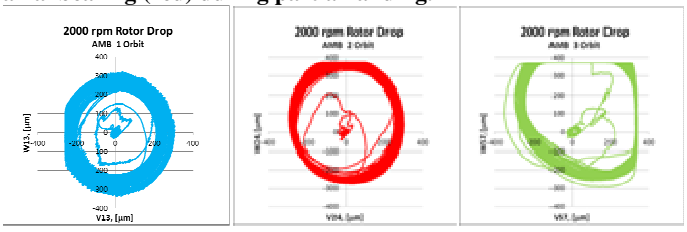

Figure 30: AMB1 (a) , AMB2 (b) and AMB3 (c) rotor orbits (1µm=0.04mils) during rotor partial landing test at 2000rpm

Upon reestablishing the correct sensor parameters, the five drop sequence was finally initiated.

The main insights gained from the drop sequence are summarized below:

1) The rotor whirl frequency was forward and equal to 43 Hz at its peak value after approximately 1 second from the delevitation event;
2) A correlation between the axial load dynamics and the whirl frequency was detected; the whirl frequency increased as the axial load increased at a certain time in the coast-down;
3) The whirl amplitude exceeded the air gap of the auxiliary bearings and damping system compliance, confirming that the auxiliary bearings and supports compliance need to be accounted to predict reasonable vibration amplitudes and set proper internal clearance of the machine.

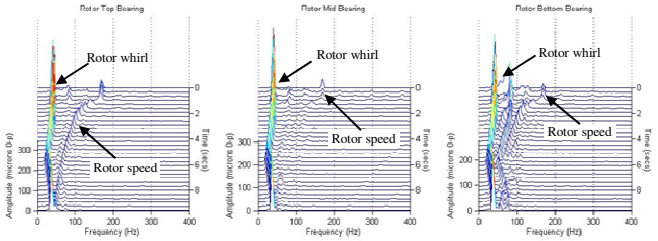

Figure 31: Vibration Waterfall Plot (1µm=0.04mils) on AMB1 (a), AMB2 (b) and AMB3 (c) during rotor drop from 10160rpm.

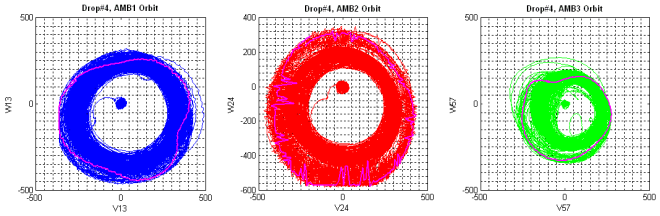

Figure 32: Vibration Orbits Plot (1µm=0.04mils) on AMB1 (a), AMB2 (b) and AMB3 (c) during rotor drop from 10160rpm.

A detailed description of the rotordynamics during the delevitation event and a comparison with the simulation is given in Masala et al. 2011.

Due to the repeatability of the drop measurements and check parameters, indicating no meaningful deviation from the 1st drop, together with the vibration amplitude and frequency being bounded within acceptable limits, the five drop tests were successfully completed.

Upon disassembling of the machine, the auxiliary bearings, landing sleeves and machine internal parts were thoroughly inspected to identify possible wear experienced during the rotor drop.

The visual and laboratory analysis performed on the auxiliary bearings confirmed very good health of these bearings, with evidence of partial degradation of the dry lubricant film on the balls but no significant of material loss or overheating. The auxiliary bearing races and landing sleeves were smooth and showed limited scratches on the radial and axial contact areas.

The inspection of the machine internal parts, as depicted in Figure 34 confirmed that no contact between the rotor and the seals had occurred during the landing tests and the correct setting of the internal clearance for optimized performance and

preservation during machine operation even in case of a delevitation event.

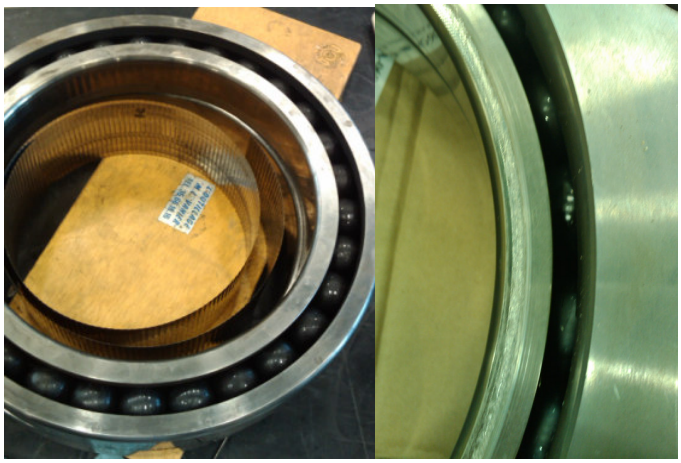

(a) (b)

Figure 33: Mid-span radial auxiliary bearing (a) and detail of the axial contact area on top auxiliary bearing (b)

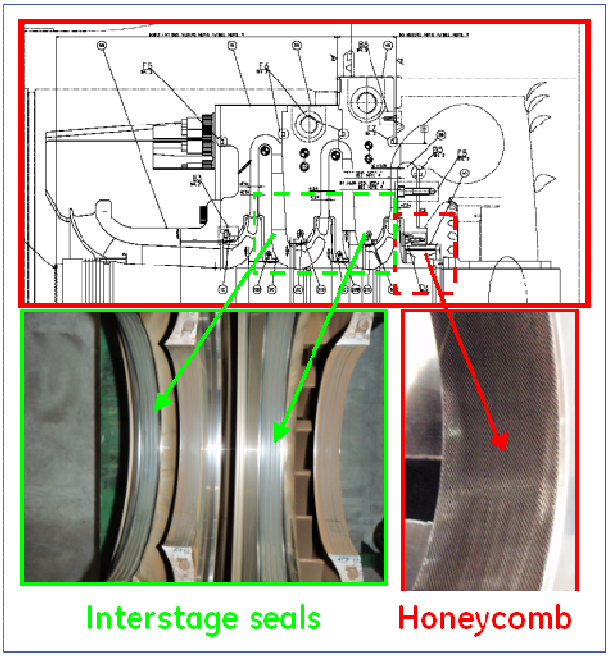

Figure 34: Interstage labyrinth seals (a) and balance drum honeycomb seal (b) upon inspection.

As a result of the landing tests and following the inspection, the rotor and auxiliary bearings demonstrated the capability of the machine to survive a minimum of five full speed emergency landings without noticeable damage. The test performed also highlighted the importance of setting up robust and coordinated procedures for the performance of the landing test and handling the performance indicators generated during repeated drop tests.

CONCLUSIONS

This paper shows in detail the results of the full load test performed at the Authors' Company facility on the motorcompressor prototype for subsea compression applications.

The test campaign allowed the fully evaluation of the machine performance (thermodynamics, rotordynamics, system cooling etc.) and demonstrated satisfactory behaviour. The test revealed both the very positive aspects of this prototype (compressor and electric motor performance, landing, control system) and areas for potential improvement (axial load and system cooling). The test results collected by the design team will be a source of validation of the predictive tools used and the starting point for improving the next project.

The next step will be the Extended Factory Acceptance Test to be performed at the costumer's site (Nyhamna) starting in the second half of 2011.

NOMENCLATURE

AMB = Active Magnetic Bearing
EM: Electric Motor
FAT = Factory Acceptance Test
MCS: Maximum Continuous Speed
mos: minimum operating speed

REFERENCES

D. Ransom, A. Masala, G. Vannini, J. Moore, M. Camatti, M- Lacour, 2009, "Development and Application of a Vertical High Speed Motor-Compressor Simulator for Rotor Drop onto Auxiliary Bearings", Proceedings of 38th Turbomachinery Symposium, Turbomachinery Laboratory, Texas A&M University, College Station Texas, pp. 1-12.

A. Masala, G. Vannini, M. Lacour,, F.-M. Tassel, M. Camatti, 2010, Lateral rotordynamic analysis and testing of a vertical high speed 12.5MW motorcompressor levitated by Active Magnetic Bearings, 12th International Symposium on Magnetic Bearings, Wuhan, China.

A. Masala, G. Vannini, D. Ransom, J. Moore, Numerical simulation and full scale landing test of a 12.5 MW vertical motorcompressor levitated by active magnetic bearings, 2011, ASME TurboExpo, Vancouver, Canada.

API 617 7th Edition, 2001: Axial and Centrifugal Compressors and Expander-Compressors for Petroleum, Chemical and Gas Industry Services, Seventh Edition, American Petroleum Institute, Washington, D.C.

ACKNOWLEDGEMENTS

The authors thank GE Oil&Gas for allowing the publication of this work.

Special thanks go to all the people who helped to make this project real both from the GE side and from the main Suppliers side (SKF/S2M as AMBs supplier and CONVERTEAM Motor as Electric Motor Supplier).

Finally, we respectfully thank our direct customer (AkerSolutions) and our final customers (Statoil and Shell) for their patience during the difficult times and for all the trust they placed in us, which we hope was rewarded by the final delivery of the unit.